Analytical Methods

ROYAL SOCIETY OF CHEMISTRY

PAPER

View Article Online
View Journal | View Issue

Check for updates

Cite this: *Anal. Methods*, 2025, **17**, 2321

Development of amide-based molecular cages for the highly selective and sensitive detection of nicotine†

Mina Bagherifard, Amrit Kaur, Kamal E. S. Nassar, Neelam Tariq, Zois Syrgiannis and Ioannis Spanopoulos *

Received 6th February 2025
Accepted 11th February 2025

DOI: 10.1039/d5ay00206k

rsc.li/methods

Nicotine is a harmful sympathomimetic drug associated with serious health issues. Herein, a novel amide-based bistren-type cage, **BiP-Am**, has been developed for the selective fluorescence-based sensing of nicotine in human urine samples and cigarettes. The corresponding detection limit features a value of 0.4 nM, among the best reported in the literature. Selectivity experiments demonstrate that **BiP-Am** can efficiently detect nicotine in the presence of multiple interfering analytes such as sodium, potassium, urea and uric acid. A plausible mechanism has been proposed herein, revealing that nicotine is showing an inner-filter effect quenching the **BiP-Am** fluorescence emission. Our strategy poses a facile and versatile method for nicotine detection in portable applications.

Open Access Article. Published on 21 February 2025. Downloaded on 1/21/2026 6:54:07 PM.
This article is licensed under a Creative Commons Attribution-NonCommercial 3.0 Unported Licence.

Introduction

Nicotine is the primary alkaloid found in the tobacco plant, featuring a major role in tobacco addiction.[1] The human body can be exposed to nicotine *via* active and passive smoking of cigarettes (including e-cigarettes), cigars, and other tobacco-based products.[2,3] The consumption of nicotine has adverse effects on human health and can promote the development of cardiovascular diseases, cancer, Alzheimer's disease, Parkinson's disease, Tourette syndrome, and various respiratory disorders.[4–7] It has been reported that as little as 0.5–1 mg of nicotine per kg of body weight in adults can be fatal.[8] Considering the above, it is of paramount importance to develop efficient, selective, and reliable methods for the facile detection and monitoring of nicotine in human fluids, such as urine, saliva, and serum.[9–11]

To this end, several analytical methods have been developed for detecting nicotine, such as gas chromatography (GC), high-performance liquid chromatography (HPLC), radioimmunoassay, capillary electrophoresis, electrochemiluminescence (ECL), and surface-enhanced Raman spectroscopy (SERS).[12–15] HPLC is the most frequently employed technique for the quantitative analysis of nicotine in biological samples.[16] Despite their efficiency, the aforementioned techniques require intricate pretreatment protocols, costly and heavy equipment, and highly skilled trained operators.[17] Therefore, emerging technologies that enable facile, highly selective, and sensitive nicotine detection without the use of expensive and complex equipment are greatly sought after, especially for portable applications. Evidently, fluorescence-based detection is rapid, non-invasive, selective, and highly sensitive, enabling easy real-time monitoring without a lengthy sample preparation process.[18] Consequently, a tailor-made fluorescence-based nicotine sensor poses an excellent choice for detecting trace amounts of nicotine in various samples, such as e-liquids, wastewater, and biological fluids, to name a few.[19,20]

To date, various fluorescence-based probes, such as metal–organic frameworks (MOFs), carbon nanodots, and metalloporphyrins (Table S1, ESI†), have been developed to detect nicotine.[21–23] Although these probes have several advantages as tools for molecular recognition, their complex and expensive synthesis and composition of toxic elements limit their widespread utilization.[9,24] Notably, fully organic molecular cages have garnered significant research interest due to their wide applications in gas storage, catalysis, sensing, and guest binding.[25] In recent years, the development of water-soluble cages based on pyridinium cations, acyl hydrazone polyamides, urea cages, heterodimeric disulfide cages, imidazolium cages, and imine cages has enabled them to be widely applied in the field of molecular recognition.[26,27] Amide cages are widely used for the molecular recognition of biomolecules such as carbohydrates, amino acids, and amines.[28–31] Even though significant progress has been made, the majority of reported methods—particularly those involving irreversible bonds—entail challenging features such as template-based synthesis, multistep reactions, limited yields, and laborious purification methods.[32] These characteristics hinder their widespread utilization for scalable real-life applications.

Department of Chemistry, University of South Florida, Tampa, Florida 33620, USA. E-mail: spanopoulos@usf.edu

† Electronic supplementary information (ESI) available. See DOI: https://doi.org/10.1039/d5ay00206k

Open Access Article. Published on 21 February 2025. Downloaded on 1/21/2026 6:54:07 PM.
This article is licensed under a Creative Commons Attribution-NonCommercial 3.0 Unported Licence.

Motivated by the above, we report herein the facile synthesis of a novel amide-based bistren cage, namely **BiP-Am.** Utilization of a Schiff base condensation reaction followed by a Pinnick oxidation step gave rise to the corresponding cage **BiP-Am**, which is reported for the first time in literature. It is expected that the introduction of multiple amide functional groups (six per molecule) coupled with aromatic moieties will enable the probe to interact with the analyte (nicotine) *via* extensive hydrogen bonding and π–π stacking, thus maximizing analyte–probe interactions. Evidently, the developed amide cage **BiP-Am**, owing to hydrophobic interactions and π–π stacking, exhibited aggregation-induced emission enhancement (AIEE) under light activation. Interestingly, the self-assembled molecules of **BiP-Am** exhibited a "turn-off" response towards nicotine in aqueous media. The probe **BiP-Am** exhibits nicotine-induced quenching in emission due to the inner filter effect (IFE), along with enhanced π–π stacking leading to the formation of closely packed assemblies. The developed probe **BiP-Am** can efficiently detect nicotine in aqueous media with a limit of detection as low as 0.4 nM. Moreover, **BiP-Am** was deployed for real-time detection of nicotine in human urine samples and extracted commercial cigarette contents in an aqueous medium. We point out that this is the first time a molecular cage has been utilized for nicotine detection, to the best of our knowledge.

Results and discussions

BiP-Am was synthesized *via* the Pinnick oxidation of the Schiff base (Scheme 1).[33] The chemical structure and purity of the **BiP-Am** was confirmed by various analytical techniques such as NMR and MALDI-TOF (Fig. S1–S5, ESI†).

Following the confirmation of the chemical structure of the probe molecule, we evaluated its optical properties. The absorption and emission spectra of the **BiP-Am** cage were examined in the presence of various solvents, such as tetrahydrofuran (THF), dichloromethane (DCM), acetonitrile (ACN), and methanol (MeOH) at room temperature. The absorption spectra (Fig. S6A, ESI†) show that polar protic solvents can stabilize the **BiP-Am** probe in its ground state. The emission spectra recorded upon varying the solvent polarity under excitation at 273 nm (Fig. S6B, ESI†) revealed that polar protic solvents such as MeOH can cause significant quenching along with a blue shift in the emission spectra in comparison with polar aprotic solvents such as DCM.[34]

Upon successive addition of water fractions, up to 99% in a solution containing **BiP-Am** in DMSO, an increase in the absorbance intensity is observed along with a slight red shift of the recorded spectra (Fig. S7A, ESI†). As depicted in Fig. S7B, ESI† the emission spectrum of the **BiP-Am** in H_2O : DMSO (9.9 : 0.1, v/v, 10 μM) exhibited an intensity enhancement along with a blue shift from 426 nm in pure DMSO ($\Phi = 2.13\%$) to 410 nm in H_2O : DMSO (9.9 : 0.1, v/v, 10 μM) ($\Phi = 5.46\%$) at an excitation wavelength of 273 nm, which suggests the formation of aggregation-induced emission enhancement (AIEE).

Upon addition of nicotine (1 mM) to a **BiP-Am** solution (H_2O : DMSO, 9.9 : 0.1, v/v, 10 μM), the absorption intensity of the probe decreases along with the appearance of a red-shifted absorption band of nicotine at 265 nm (Fig. S8, ESI†). As shown in Fig. 1, photoluminescence (PL) studies revealed an acceptable quenching (Φ = 3.04%) upon the addition of nicotine (1 mM) into the H_2O : DMSO (9.9 : 0.1, v/v, 10 μM) solution of the **BiP-Am**, with a quenching efficiency of 77% (Fig. 2A). Quenching efficacy was calculated by using $QE = 1 - (F/F_0)$ formula; F_0 represents the fluorescence intensity measured prior to the addition of nicotine to the H_2O : DMSO (9.9 : 0.1, v/v, 10 μM) solution, while F represents the fluorescence intensity measured after nicotine is added.

In Fig. 1, the effect of different nicotine concentrations on the **BiP-Am** probe emission spectra is presented. The limit of detection (LOD) was calculated using the formula $LOD = \frac{3\sigma}{m}$, where σ represents the standard deviation of the signal and m denotes the slope of the calibration curve. The LOD was determined to be approximately 0.4 nM (when σ is 0.008), demonstrating the probe's excellent sensitivity for detecting nicotine in

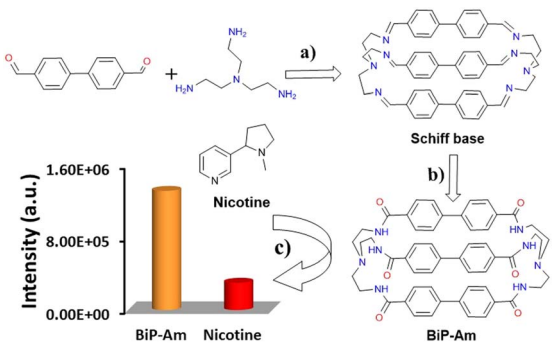

Scheme 1 The synthetic route of the **BiP-Am** cage: (a) 4.8 mmol of [1,1′-biphenyl]-4,4′-dicarbaldehyde, 3.2 mmol of tris(2-aminoethyl) amine, 275 mL of ACN, 0 °C, 7 days. (b) 0.6 mmol of Schiff base, 20.1 mmol of sodium chlorite, 7.4 mmol of ammonium chloride, and 36.8 mmol of (1*S*)-(−)-α-pinene, 100 mL of dry THF under reflux for 48 hours. (c) The interaction of the **BiP-Am** probe with nicotine solution results in a sharp decrease in the intensity of the emission spectra when excited at 273 nm.

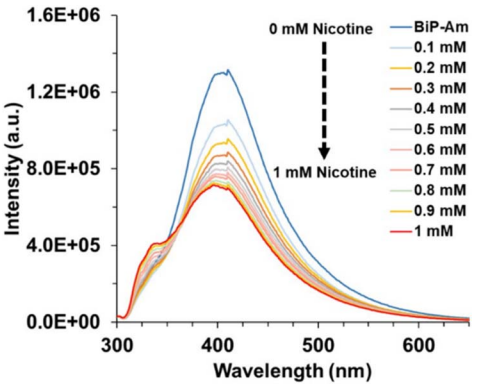

Fig. 1 Emission spectra evolution of the **BiP-Am** probe *via* successively adding 1 mM nicotine solution to a H_2O : DMSO (9.9 : 0.1, v/v, 10 μM) sample.

 This journal is © The Royal Society of Chemistry 2025

Open Access Article. Published on 21 February 2025. Downloaded on 1/21/2026 6:54:07 PM.
This article is licensed under a Creative Commons Attribution-NonCommercial 3.0 Unported Licence.

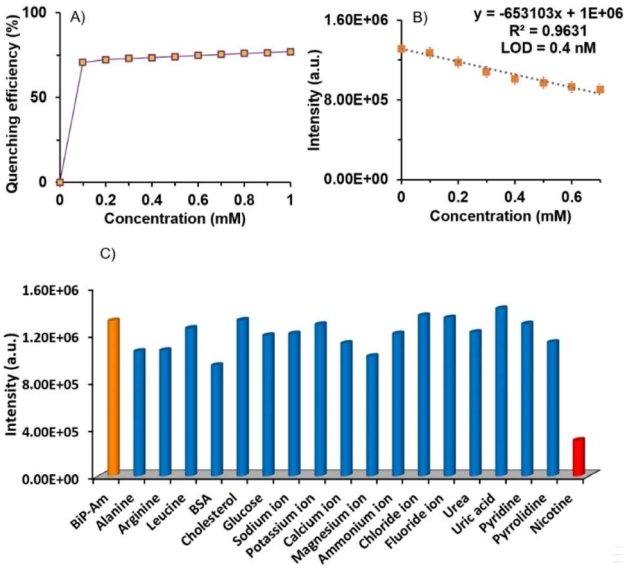

Fig. 2 (A) PL quenching efficiency of **BiP-Am** probe (H_2O : DMSO (9.9 : 0.1, v/v, 10 μM)) upon addition of 0.1 mM nicotine solution into 3 mL probe solution; (B) calibration curve for **BiP-Am** probe response to the addition of 0.1 mM Nicotine solution; and (C) the emission intensity of pure **BiP-Am** in H_2O : DMSO (9.9 : 0.1, v/v, 10 μM) (orange column) and its response upon the addition of various interferents (blue and red columns) are presented. Nicotine significantly quenched the **BiP-Am** probe emission.

diluted samples (Fig. 2B). Notably, this is among the best-reported values in literature (Table S1†).

Selectivity studies of **BiP-Am** probes were performed in the presence of potential interfering analytes such as Na^+, K^+, Ca^{2+}, Mg^{2+}, NH_4^+, Cl^-, F^-, alanine, arginine, leucine, bovine serum albumin (BSA), glucose, cholesterol, urea, uric acid, pyridine, pyrrolidine, and nicotine. The concentration of all interferents was 1 mM and a negligible quenching effect was observed in the presence of these analytes except for nicotine (Fig. 2C). This performance demonstrated the excellent selectivity of the probe molecule and its potential for utilization in real-world samples.

Toward this end, for real-time evaluation of **BiP-Am** in biological samples such as urine, we carried out competitive experiments in the presence of all the above-mentioned interfering analytes by setting their concentration to 1 mM, in the presence of 1 mM nicotine. As shown in Fig. S9, ESI,† nicotine addition in the presence of interfering analytes quenches PL intensity indicating the strong selectivity of the probe towards nicotine.

A Stern–Volmer diagram is depicted in Fig. S10, ESI,† showing the ratio of sample PL intensity before and after the addition of the quencher *versus* the quencher's concentration, $F_0/F = K[Q] + 1$. Here, F_0 is the fluorescence intensity before the addition of nicotine to the solution H_2O : DMSO (9.9 : 0.1, v/v, 10 μM), and F is the fluorescence after the addition of nicotine, K is the quenching constant, and [Q] is the quencher's concentration. The linear dependence ($R^2 = 0.953$) of the ratio F_0/F on the quencher concentration suggests the dynamic nature of quenching. The slope of the linear regression between F_0/F and [nicotine] gave a value of $K = 0.6\ mM^{-1}$.

To evaluate the excited state interactions, we carried out time-resolved photoluminescence (TRPL) studies with an excitation wavelength of 300 nm (Fig. S11, ESI†).[35] The time-resolved studies of **BiP-Am** in H_2O : DMSO (9.9 : 0.1, v/v, 10 μM) showed an amplitude-weighted average lifetime (τ_{amp}) and an intensity-weighted average lifetime (τ_{int}) of 6 ns and 19 ns, respectively ($\tau_1 = 1.22$ ns, 14.87%; $\tau_2 = 10.11$ ns, 22.61%; $\tau_3 = 26.47$ ns, 62.52%). Upon addition of nicotine to the **BiP-Am** solution, there was a significant decrease in both τ_{amp} and τ_{int} to 4 ns and 13 ns, respectively ($\tau_1 = 1.19$ ns, 23.84%; $\tau_2 = 9.31$ ns, 34.44%; $\tau_3 = 23.51$ ns, 41.72%), suggesting that the quenching mechanism is primarily dynamic.

Moreover, to get an insight into the molecular interaction between nicotine and **BiP-Am**, we carried out ^1H NMR studies in DMSO-d_6 : D_2O (9 : 1, v/v). It was revealed that the aromatic protons of the **BiP-Am** exhibited a slight upfield shift (0.008 ppm) (Fig. S12, ESI†). This suggests potential nicotine-induced enhanced π–π or hydrogen bond interactions of the analyte with the probe molecules. Furthermore, dynamic light scattering (DLS) results revealed an aggregation upon the addition of nicotine to the **BiP-Am** sample (H_2O : DMSO (9.9 : 0.1, v/v)), while the particle size changed from 825 nm to 1345 nm (Fig. S13, ESI†). The induced aggregation upon the addition of nicotine solution to the **BiP-Am** sample was analyzed by scanning electron microscopy (SEM). The **BiP-Am** probe SEM image in Fig. 3A shows dispersed spherical-shaped particles, which form closely packed aggregates in the presence of nicotine (Fig. 3B), corroborating further the strong interaction among the probe molecules in the presence of the analyte.

In order to demonstrate the mechanism of action in the detection of nicotine by the probe molecules, we performed the following experiments. The emission spectra of the **BiP-Am** probe in the presence of nicotine at different excitation wavelengths, from 233 nm to 313 nm, were carried out. It was observed that by changing the excitation wavelength, a variation in emission intensity was recorded, while no change in λ_{max} was detected (Fig. S14, ESI†), suggesting an IFE mechanism of action.[36]

The absorption spectrum of nicotine recorded in H_2O : DMSO (9.9 : 0.1, v/v, 10 μM) displayed a narrow absorption band from 250–300 nm with λ_{max} at 260 nm, which barely overlaps with the emission spectrum of probe **BiP-Am** ranging from 300–650 nm with λ_{max} at 410 nm (Fig. S15A, ESI†). Simultaneously,

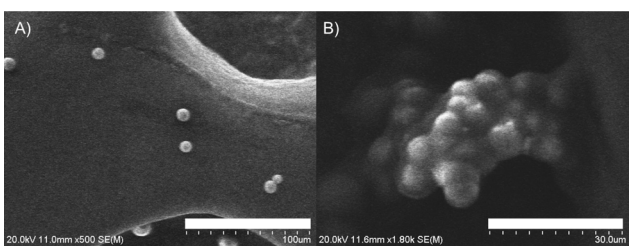

Fig. 3 SEM images of (A) the **BiP-Am** sample at 100 μm scale and (B) the BiP-Am-nicotine aggregate at 30 μm scale.

Open Access Article. Published on 21 February 2025. Downloaded on 1/21/2026 6:54:07 PM.
This article is licensed under a Creative Commons Attribution-NonCommercial 3.0 Unported Licence.

Table 1 Nicotine detection in real-world samples

Sample	Detected nicotine (mM)	Added nicotine (mM)	Found (mM)	STD (%)	RSD (%)
Cigarette	0.208			0.03	0.17
Spike 1		0.500	0.723	0.04	0.08
Spike 2		0.700	0.901	1.03	1.50
Urine	Not detected				
Spike 1		0.300	0.326	0.45	1.49
Spike 2		0.500	0.512	0.27	0.54

upon analysis, the emission spectrum of nicotine, which ranges from below 300 to 600 nm slightly overlaps with the **BiP-Am** probe absorption spectrum 250–360 nm with λ_{max} at 273 nm (Fig. S15B, ESI†). These results rule out FRET as a possible mechanism in this system.

Density Functional Theory (DFT) and Time-Dependent Density Functional Theory (TDDFT) calculations, employing the B3LYP functional with the 6-31G(d) basis set, were conducted to investigate the possibility of photo-induced electron transfer in the **BiP-Am** probe upon excitation. The results, summarized in Table S2, ESI,† indicate that such a transfer is unlikely, as the excited-state HOMO energy level of **BiP-Am** (−5.029 eV) is higher than the ground-state HOMO energy level of nicotine (−5.508 eV). This energy difference suggests that electron transfer from nicotine to **BiP-Am** is not energetically favorable.

In order to demonstrate the potential of our probe molecule in real-world samples, we utilized **BiP-Am** for the detection of nicotine in human urine samples and extracted nicotine solutions from cigarettes. The cigarette samples were diluted in distilled water, followed by sonication, centrifugation, and filtration to obtain a clear solution. The nicotine content in cigarettes, calculated using the standard calibration method without spiking, was found to be 0.208 mM. We further spiked the cigarette solution with standard nicotine solution (0.500 and 0.700 mM) and calculated the amount of nicotine using the calibration curve. Examining closely the cigarette and 0.500 mM spike case, we determined an amount of 0.723 mM, very close to the total expected one (0.500 + 0.208 = 0.708). Apparently, the determined amounts matched the actual nicotine amounts pretty well, demonstrating the robustness of the method (Fig. S16A, ESI†).

Considering the human urine sample analysis, a 100-fold dilution was performed before the quantification of the nicotine content. The urine samples were also spiked with a known concentration of nicotine (0.300 and 0.500 mM), while a standard calibration curve was used to identify the spiked nicotine concentration (Table 1). Notably, the relative standard deviation was found to be less than 1.5%, while the determined amount matches very closely the spiked amount (*e.g.* 0.500 mM *vs.* 0.512 mM, Fig. S17B, ESI†). These results suggest that the **BiP-Am** probe holds potential for the selective and efficient detection of nicotine in real-world samples, such as human urine and cigarettes. Further modifications and optimizations could enhance its performance and broaden its practical applications.

Conclusion

In conclusion, we designed and synthesized a new amide-based cage, namely **BiP-Am**, and utilized it as a probe to detect nicotine in aqueous media with excellent selectivity and sensitivity. The corresponding detection limit lies in the nanomolar range, among the best reported in the literature, making it suitable for real-time applications. TRPL and DFT studies confirmed the dynamic quenching mechanism primarily due to the inner-filter effect of nicotine. Further validation through ^{1}H NMR studies, dynamic light scattering, and SEM measurements provided insight into the molecular interactions and aggregation behaviour of the **BiP-Am** probe in the presence of nicotine. The probe was effectively applied to detect nicotine in real samples, including cigarette extracts and human urine, showcasing its potential for practical applications. Our findings suggest that **BiP-Am** has the potential to serve as a foundation for developing a more effective sensor for nicotine detection.

Data availability

The data supporting this article have been included as part of the ESI.†

Conflicts of interest

There are no conflicts to declare.

Acknowledgements

We acknowledge financial support from USF start-up funds. We also acknowledge support from the USF Student Health & Wellness Center for providing the urine samples, with special thanks to Dr Joseph Puccio, Dr Aileen Cannon, and Dr Danielle Morris. We also appreciate the assistance of Dr Chavdar Slavov, and Dr Wayne Guida for providing access to their equipment.

Notes and references

1 B. Le Foll, M. E. Piper, C. D. Fowler, S. Tonstad, L. Bierut, L. Lu, P. Jha and W. D. Hall, *Nat. Rev. Dis. Primers*, 2022, **8**, 19.
2 P. Marques, L. Piqueras and M.-J. Sanz, *Respir. Res.*, 2021, **22**, 151.
3 L. S. Flor, J. A. Anderson, N. Ahmad, A. Aravkin, S. Carr, X. Dai, G. F. Gil, S. I. Hay, M. J. Malloy, S. A. McLaughlin,

 This journal is © The Royal Society of Chemistry 2025

Open Access Article. Published on 21 February 2025. Downloaded on 1/21/2026 6:54:07 PM.
This article is licensed under a Creative Commons Attribution-NonCommercial 3.0 Unported Licence.

E. C. Mullany, C. J. L. Murray, E. M. O'Connell, C. Okereke, R. J. D. Sorensen, J. Whisnant, P. Zheng and E. Gakidou, *Nat. Med.*, 2024, **30**, 149–167.
4 B. Lin, J. Chen, Y. Zeng, L. Li, B. Qiu, Z. Lin and L. Guo, *ACS Sens.*, 2019, **4**, 1844–1850.
5 P. A. Newhouse, A. Potter, M. Kelton and J. Corwin, *Biol. Psychiatry*, 2001, **49**, 268–278.
6 A. Alhowail, *Mol. Med. Rep.*, 2021, **23**, 1–6.
7 G. K. Lloyd and M. Williams, *J. Pharmacol. Exp. Ther.*, 2000, **292**, 461–467.
8 S. Mondal, I. Ahmad and N. Dey, *ACS Appl. Bio Mater.*, 2024, **7**, 2346–2353.
9 Z. Hu and B. Yan, *J. Mater. Chem. A*, 2023, **11**, 4739–4750.
10 A. N. Ramdzan, M. I. G. S. Almeida, M. J. McCullough, M. A. Segundo and S. D. Kolev, *TrAC, Trends Anal. Chem.*, 2018, **105**, 89–97.
11 F. Soleimani, S. Dobaradaran, G. E. De-La-Torre, T. C. Schmidt and R. Saeedi, *Sci. Total Environ.*, 2022, **813**, 152667.
12 O. Gould, N. Nguyen and K. C. Honeychurch, *Chemosensors*, 2023, **11**, 527.
13 A. Marsh, B. J. Clark and K. D. Altria, *Electrophoresis*, 2004, **25**, 1270–1278.
14 A. Karthika, P. Karuppasamy, S. Selvarajan, A. Suganthi and M. Rajarajan, *Ultrason. Sonochem.*, 2019, **55**, 196–206.
15 B. Lin, Y. Yao, Y. Wang, L. Chen, X. Peng and L. Guo, *ACS Appl. Mater. Interfaces*, 2021, **13**, 37638–37644.
16 M. Yasuda, T. Ota, A. Morikawa, K.-I. Mawatari, T. Fukuuchi, N. Yamaoka, K. Kaneko and K. Nakagomi, *J. Chromatogr. B*, 2013, **934**, 41–45.
17 A. E.-G. E. Amr, A. H. Kamel, A. A. Almehizia, A. Y. A. Sayed, E. A. Elsayed and H. S. M. Abd-Rabboh, *ACS Omega*, 2021, **6**, 11340–11347.
18 K. Liu, J. Zhang, L. Xu, J. Liu, L. Ding, T. Liu and Y. Fang, *Chem. Commun.*, 2019, **55**, 12679–12682.
19 N. Cennamo, G. D'Agostino, M. Pesavento and L. Zeni, *Sens. Actuators, B*, 2014, **191**, 529–536.
20 J. Wu, W. Liu, J. Ge, H. Zhang and P. Wang, *Chem. Soc. Rev.*, 2011, **40**, 3483.
21 D. Yan, Y. Lou, Y. Yang, Z. Chen, Y. Cai, Z. Guo, H. Zhan and B. Chen, *ACS Appl. Mater. Interfaces*, 2019, **11**, 47253–47258.
22 X. Xu, Z. Chen, Q. Li, D. Meng, H. Jiang, Y. Zhou, S. Feng and Y. Yang, *Microchem. J.*, 2021, **160**, 105708.
23 G. R. Deviprasad and F. D'Souza, *Chem. Commun.*, 2000, 1915–1916.
24 C. Yang and B. Yan, *Inorg. Chem.*, 2023, **62**, 20458–20466.
25 S. La Cognata and V. Amendola, *Chem. Commun.*, 2023, **59**, 13668–13678.
26 W. Liu, Y. Tan, L. O. Jones, B. Song, Q.-H. Guo, L. Zhang, Y. Qiu, Y. Feng, X.-Y. Chen, G. C. Schatz and J. F. Stoddart, *JACS*, 2021, **143**, 15688–15700.
27 H. Li, H. Zhang, A. D. Lammer, M. Wang, X. Li, V. M. Lynch and J. L. Sessler, *Nat. Chem.*, 2015, **7**, 1003–1008.
28 K. G. Andrews and K. E. Christensen, *Chem.–Eur. J.*, 2023, **29**, 26.
29 L. Tapia, I. Alfonso and J. Solà, *Org. Biomol. Chem.*, 2021, **19**, 9527–9540.
30 X. Yang, Z. Ullah, J. F. Stoddart and C. T. Yavuz, *Chem. Rev.*, 2023, **123**, 4602–4634.
31 J. C. Lauer, A. S. Bhat, C. Barwig, N. Fritz, T. Kirschbaum, F. Rominger and M. Mastalerz, *Chem.–Eur. J.*, 2022, **28**, e202201527.
32 S. Maji, J. Samanta and R. Natarajan, *Chem.–Eur. J.*, 2024, **30**, 1–9.
33 M. Boiocchi, M. Bonizzoni, L. Fabbrizzi, G. Piovani and A. Taglietti, *Angew. Chem., Int. Ed.*, 2004, **43**, 3847–3852.
34 E. Fresch and E. Collini, *Molecules*, 2023, **28**, 3553.
35 Q. Zhang, Y. Sun, M. Liu and Y. Liu, *Nanoscale*, 2020, **12**, 1826–1832.
36 P. Sharma, M. Kumar and V. Bhalla, *ACS Omega*, 2020, **5**, 19654–19660.